Spectrum of Engineering Sciences
ISSN (e) 3007-3138 (p) 3007-312X Volume 3, Issue 12, 2025

GENERATIVE ADVERSARIAL NETWORKS FOR IMAGE RESTORATION IN LOW-LIGHT CONDITIONS

Muhammad Zarar, [2]Talha Nadeem, [3]Huzaifah Bin Khawar, [4] Hood Khizer
[1] AI Researcher, Research and Development Department, Trouve Labs, AHOY DMCC and The Superior University Lahore, Pakistan muhammadzarar.ieee@gmail.com
[2] Systems Architect AI/ML, Research and Development Department, Trouve Labs, AHOY DMCC and The Superior University Lahore, Pakistan talhanadeem.ieee@gmail.com
[3] AI Researcher, Research and Development Department, Trouve Labs, AHOY DMCC and The Superior University Lahore, Pakistan huzaifahkhawar.ieee@gmail.com
[4] CEO Trouve Labs, CTO AHOY DMCC, Research and Development Department, Trouve Labs, AHOY DMCC, Dubai hoodkhizer@gmail.com

DOI:https://doi.org/10.5281/zenodo.24117254

Keywords
Generative adversarial networks, low-light image enhancement, hybrid attention module, parallel dilated convolution module.

Article History
Received: 10 Sep, 2025
Accepted: 18 Dec, 2025
Published: 27 Dec, 2025

Copyright @Author
Corresponding Author: *
Talha Nadeem*

Abstract

Low-light image enhancement aims to improve the perceptual quality of images captured under low-light conditions. This paper proposes a novel generative adversarial network to enhance low-light image quality. Firstly, it designs a generator consisting of residual modules with hybrid attention modules and parallel dilated convolution modules. The residual module is designed to prevent gradient explosion during training and to avoid feature information loss. The hybrid attention module is designed to make the network pay more attention to useful features. A parallel dilated convolution module is designed to increase the receptive field and capture multi-scale information. Additionally, a skip connection is utilized to fuse shallow features with deep features to extract more effective features. Secondly, a discriminator is designed to improve the discrimination ability. Finally, an improved loss function is proposed by incorporating pixel loss to effectively recover detailed information. The proposed method demonstrates superior performance in enhancing low-light images compared to seven other methods.

I. INTRODUCTION

Under low illuminations conditions (when weather is cloudy and at night), the captured images have low brightness, noise intensity and color distortion. All of these have profound effects on any high-level vision task, such as image segmentation and object detection. In such instances it is essential to improve the low-light image to ensure the accuracy

of such tasks. The most commonly used traditional methods to enhance images taken under low light are histogram equalization and Retinex. Histograms equalization is one of the several global contrast enhancement techniques which can be used by stretching the distribution of the image's histogram. It can make background noise louder and diminish the contrast in useful information, however. Moreover, it may also lead to oversaturated and detailed information loss. The other side, Retinex theory method, assumes that the illumination should be removed from the original image to obtain the enhanced image. But it can also produce "halo" effects, notably in shots where light levels are different, that alter a picture's quality. Due to the development of deep-learning technologies, deep-learning based low-light image enhancement (LIH) has been proposed. A large number of methods make use of paired image data to train the network and also to acquire the model that can afterwards be utilized for improving the low-light images. The following are techniques that demand low light images and original high-definition images. The acquisition of paired images in typical applications, however, is a difficult task. Therefore, low-light image enhancement methods based on generative adversarial networks (GANs) unsupervised enhancement methods were proposed. The above methods do not use matched images for training and would be more useful in practice.

In order to improve the quality of enhanced pictures, by using unsupervised learning, we present a generative adversarial network (GAN) for low light image enhancement. This is a network consisting of the generator and the discriminator. The generator generates a good image and the discriminator decides whether not an image is a generated high quality image, or an original high quality image. Using the generator and discriminator together allows us to improve the image generation ability of the generative network. The output of the discriminator is used to adjust the parameters of both networks. The adversarial network positions itself to be unable to tell between generated images and images of its own they are trained through an iterative process. After training, the trained generator is then applied to improve the low-light images.

In this paper, the main contributions such as designing a novel generator for improving the low-light image are summarized. First, we developed a hybrid attention module with an "attention" accelerator channel attention module and a pixel attention module.Firstly, a hybrid attention module with channel attention module and an "attention" pixel attention module were developed. Secondly, we used the hybrid attention module as a sub-module of the residual module design. Thirdly, we did design a parallel dilated convolution module to obtain multiscale information. Finally, we merged the aforementioned designed residual module with the hybrid attention module and parallel dilated convolution module to build the generative network. Furthermore, we used a skip connection as a fusion between shallow and deep features to improve capability of the generative network.

We suggest that the adversarial network has two discriminators: one at the global level, and the other at the local level. Multi-layer per stage discriminator models consisting of 6 standard convolutions in the local discriminator and 3 dilated

convolutions in the global discriminator with skip connections and 4 standard convolutions are used.

We suggest an improved loss function by incorporating the pixel loss in the loss function of the generative adversarial network. It works well on recovering more detailed image information.

Section 2 reviews related work. Section 3 presents the mathematical notation, generator, discriminators, loss functions, and training and inference algorithms. Section 4 reports the datasets, evaluation metrics, ablation results, and comparative analyses. Section 5 concludes the paper.

II. RELATED WORK

Over the last few years, a wide variety of schemes have been suggested for the enhancement of low light images. Such approaches can be broken down into traditional and deep learning techniques. The Traditional methods may be further divided into two types: low-light image enhancement using histogram, low-light image enhancement using Retinex theory. Based on histogram equalization, low-light image enhancement is a technique which performs an enhancement on the image, in order to improve the histogram distribution characteristics of the image, to change the gray value of the picture, thus to improve the performance of the image. But pictures taken with this technique have too much noise, colour distortion and loss of detailed information. Low-light image enhancement method based on Retinex theory: The method works by estimating the illumination component of the image, and subtracting it from the image to enhance low-quality images. This, however, does not take account of the effect of noise in the reflectance, thus creating artifacts and overexposures in the resulting image.

With the advancement of deep-learning techniques, a multitude of low-light image enhancement methods have been developed based on deep-learning approaches. These methods have been found to have better performance in improving image quality than the traditional methods. For example, the information from a picture is decomposed using a data-driven method named Retinex-Net into illumination and reflectance. Addressing the problem of noise interference in the reflectance component, the BM3D method is used, which in general results in better removal of noise interference in the Retinex theory-based method. An encoder-decoder network is actually applied to obtain the feature information out of the illumination part to reduce the influence of the changes of light. Under this method, however, it is difficult to retrieve color information of the image effectively.

A different way introduces to the framework a semi-supervised network based on deep recursive band network for improving low-light images. There are two phases in this network: band recomposition and recursive band learning. During the band recomposition stage, the network is trained based on the paired images: low light and normal light images. The trained network reconstruction a linear band representation of an enhanced normal-light image. The learnable linear transformations and the given bands are used in the recursive band learning stage to recover the color information in the image. Though the images produced using this method have benefits in terms of preserved detailed information, attractive contrast and color distributions, the process is not very effective at removing noise.

Instead, another approach is based on zero-reference deep curve estimation for low-light image enhancement which enacts pixel-level curve estimation by a deep convolutional network to obtain the dynamic range of the higher-order curve. One of the biggest benefits to this technique is that no paired images are used, allowing for avoidance of degradation in the images due to overfitting. The method is strongly susceptible to various parameter settings of the image, however, it requires larger training time and longer time for inference.

Generative Adversarial Networks (GAN) have been used in low-light image enhancement to further improve the quality of the enhanced image. A special class of deep-learning model has gained wide use for many applications including image denoising, image super resolution, and image classification, namely a generative adversarial network. The area of image enhancement has been the domain of association of generative adversarial networks in recent years. For instance, a multi-term perceptual loss function is used here that combines image quality assessment, content and texture in the generative adversarial network. The combination of these loss terms have the effect of minimizing artifacts in the enhanced image. While it can lead to the loss of certain color feature information, it should not lead to overall saturation issues.

An alternative way involves adding spectral normalization and color loss function to improve the network training efficacy and improve color extraction. Also, local illumination is used for training to compensate for the saturation problems in the bright region. Just this method has some difficulties when used as part of underexposure.

Another method uses a generative adversarial network along with Retinex theory. Adopt U-Net as the network model of the decomposition part and the enhancement part for this method. Considering the blurring problem of the images, the method includes a structural similarity loss. It doesn't take into account noise effects in improved pictures, though.

Generative adversarial network-based methods yields better enhanced images, but the differences between the enhanced image and the true images recorded in normal light is quite large. In enhanced images there are artifacts and noise with some areas being "under-exposed" or "over-exposed". All this affects severely the overall image quality of the enhanced images. In this paper, we present a novel approach to improve the quality of the generated results by introducing a novel generative adversarial network that overcomes these limitations. The experimental results show the feasibility of our approach in order to enhance the quality of the enhanced image.

III. PROPOSED METHOD

A. Mathematical Notation and Problem Formulation

The Symbols used in methodology, equations and algorithms have been defined in Table 1. In the enhancement framework, the low-light training image is not aligned with a pixel of a normal-light input sample [22, 34] which is in fact a normal-light training sample. Only evaluate full-reference metrics with paired references.

Table 1. Mathematical notation and its relevance to the enhancement framework.

Symbol	Definition	Methodological relevance
P	Low-light RGB image; shape 3 × H × W.	Input to the generator and content-preservation losses.
Y	Normal-light RGB training image.	Independent real sample for adversarial learning.
$\hat{R}$	Enhanced RGB output; shape 3 × H × W.	Generated image assessed by discriminators and metrics.

Symbol	Definition	Methodological relevance
G_{θ_G}	Generator parameterized by θ_G.	Maps a low-light image to an enhanced image.
$\theta_G, \theta_g, \theta_l$	Generator, global-discriminator, and local-discriminator parameters.	Separate parameter sets updated by Adam.
D_g, D_l	Global and local discriminator score functions.	Evaluate whole-image realism and patch realism.
$p_{\text{low}}, p_{\text{real}}$	Low-light and normal-light sample distributions.	Specify independent sampling in adversarial expectations.
H, W, C	Spatial height, spatial width, and feature-channel count.	Define image and feature-map dimensions.
I, A	Normalized luminance map and dark-region attention map.	A = 1 - I emphasizes dark pixels.
Lum, Norm	RGB-to-luminance conversion and normalization operators.	Construct the luminance attention map using the training preprocessing.
P_{in}	Attention-adjusted generator-network input.	P plus the broadcast dark-region attention map.
T_{θ_G}	Decoder output after the Tanh activation.	Predicts the attention-weighted residual correction.
X, X_k	Intermediate feature tensor and its kth channel.	Inputs to attention, pooling, and dilated convolutions.
H_a, C_a, P_a	Hybrid, channel, and pixel attention operators.	Select informative channels and spatial features.
$\text{Conv}, \text{Conv}_1, \text{Conv}_2$	Convolution; convolution with LeakyReLU; linear convolution.	Extract features and estimate attention weights.
σ, Pool	Sigmoid activation and global average pooling.	Produce bounded weights and channel descriptors.
$\text{DilConv}_r, r$	Dilated convolution and dilation rate.	Generator rates are 1, 3, 5; global-discriminator rates are 2, 3, 5.
$M(X)$	Parallel dilated convolution module output.	Fuses the three dilation-rate branches before a convolution.
T_ω, ω	Random patch-cropping operator and crop coordinates.	Prepare local-discriminator inputs.
$\odot$, $+$, Concat	Elementwise multiplication, elementwise sum, and channel concatenation.	Apply attention, residual sums, and encoder-decoder fusion.
L_G, L_D	Total generator loss and total discriminator loss.	Keep the two optimization objectives distinct.
$L_{G,g}, L_{G,l}$	Global and local generator adversarial losses.	Encourage normal-light whole-image and patch scores.
$L_{D,g}, L_{D,l}$	Global and local discriminator losses.	Separate real samples from generated samples.
$L_{\text{perc}}, L_{\text{pixel}}$	Perceptual content loss and pixel consistency loss.	Preserve scene features and constrain excessive pixel changes.
$\phi_{i,j}, H_{i,j}, W_{i,j}$	Frozen VGG16 feature extractor and its spatial dimensions.	Define the feature-based content-preservation loss.
m, u, v, i, j, k	Flattened pixel-channel count, spatial indices, and feature/block/channel indices.	m = 3HW for RGB pixel loss; index ranges are defined with each equation.
$B_{\text{low}}, B_{\text{real}}, b$	Independent low-light and normal-light minibatches and batch size.	b = 4 in the reported training configuration.
E, e, η_0, η_e	Total epochs, current epoch, initial and current learning rates.	E = 200; learning rate is held for 100 epochs then decayed.
β_1, β_2	Adam first- and second-moment decay coefficients.	Reported optimizer values are 0.5 and 0.999.
$\mu_1, \mu_2, \Sigma_1, \Sigma_2$	Natural/test NSS mean vectors and covariance matrices.	Define the NIQE distance between statistical models.
$J, \hat{J}, \mu_J, \sigma_J, \varepsilon$	Grayscale assessment image, MSCN coefficients, local mean/deviation, and positive stabilizer.	Define BRISQUE preprocessing; the final score uses learned regression.
$\Psi_{\text{NSS}}, f_{\text{SVR}}$	Natural scene statistics feature extraction and support-vector regression.	Convert multiscale BRISQUE features to a learned quality score.
$\text{MSE}, L_{\max}$	Mean squared error and maximum image intensity.	Define PSNR; use the same intensity scale for output and reference.
$\mu_Y, \mu_R, \sigma_Y, \sigma_R, \sigma_{YR}$	Reference/output local means, deviations, and covariance for SSIM.	Y denotes the paired reference only during full-reference evaluation.
C_1, C_2	Positive SSIM stabilizing constants.	Prevent unstable ratios in low-variance windows.

Image and feature tensors use channel-first notation. One-channel attention weights are broadcast over RGB channels; channel weights are broadcast over spatial positions. Training Y samples are unpaired, whereas evaluation Y samples must be aligned with the tested input.

For a low-light image P, the generator with parameters θ_G predicts the enhanced image $\widehat{R}$. Both tensors have three color channels and the same spatial dimensions H and W.

$$\hat{R} = G_{\theta_G}(P), \quad P, \hat{R} \in \mathbb{R}^{3\times H\times W} \tag{1}$$

The generator parameters are optimized using the composite generator objective, while each discriminator has its own objective. Unlike a paired reconstruction objective, this formulation does not require a normal-light image aligned with each training input.

$$\theta_G^* = \arg\min_{\theta_G} L_G \tag{2}$$

B. Proposed Generator

We created a generator to provide superboosting of low-light images without supervision. The architecture of our proposed generator is shown in Figure 1. To maintain the sequential conventional encoding and decoding methods that had proven to be effective in the field of image enhancement, a large number of experiments had been performed, our generator was based on this structure. The generator is made of two major parts, namely, top-down network (Part A in Figure 1), and bottom-up network (Part B in Figure 1). We used downscaling operations in the top down network in order to decrease the receptive field and size of the feature map. This can retrieve more low frequencies which give the general shape of the image. The bottom-up network, on the other hand, is a network where the size of the feature map is increased through upsampling operations that it has, enabling it to give attention to finer details of the image, that are high frequency information. In order to combine the high-frequency information and low-frequency information efficiently, we also added short connections which link the top-down / bottom-up paths. These relationships help to pass information between levels of the network, and help integrate features. We aim to model an overall framework of our generative network, as shown in Figure 1.

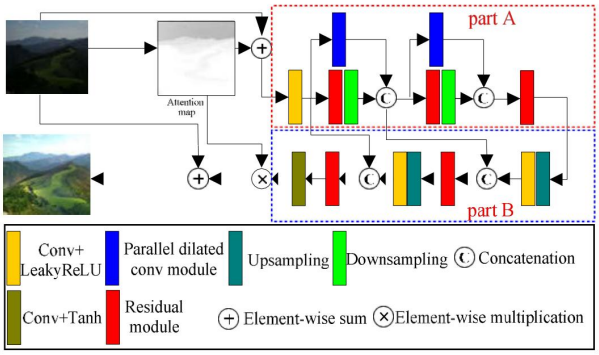


Figure 1. Generator architecture with a top-down encoder (Part A), bottom-up decoder (Part B), and skip connections.

Based on the previous work done, we carried out a pre-processing work from the original low-light image to avoid over- or under-exposed image in the output image. Firstly, we had used the luminosity method to convert RGB image to a single channel one (I) to obtain the grey level of each pixel of the image. Secondly, we have normalized the grayscale to range [0, 1] to get the luminance weight value of every pixel in the original image. Finally, the obtained image from 1-I was used as our attention map object. Note that in this attention map, larger weight values are given for the pixels located in the dark areas and smaller for the pixels in the light areas. This method enables the network to concentrate more on seeing the light portions of the image. The output is then element-wise summed with its attention map, then fed into the generative network and the result is a low-light image. We increased the number of channels from 3 to 32 by applying the learned designed network generative layers with a normal convolution layer and LeakyReLU activation function. In order to extract more useful features, we added a residual module, since adding additional time sequence layers to the original paper will not work here, we used a hybrid attention module and increased the number of

channels from 32 to 64. The first LeakyReLU activation is used as the input into the designed residual module.

Suppose that the image obtained by converting and normalizing the RGB image with a luminance function I is calculated.Suppose that a luminance image I is computed from the RGB image as described above, by a called luminance mapping and normalisation. The attention map A is more dark in dark areas. It is broadcast to the three RGB channels and elementwise added or multiplied before.

$$I = \text{Norm}(\text{Lum}(P)), \quad A = 1 - I \tag{3}$$

$$P_{\text{in}} = P + A \tag{4}$$

The decoder predicts a residual in a 3 channel Tanh, which is called T and accompanied with the generator parameters. Attention-weighted Residual Reconstruction maintains the connection to the original input:

$$\widehat{R} = P + A \odot T_{\theta_G}(P_{\text{in}}) \tag{5}$$

To obtain the low frequency information we downsampled the output of the residual module. Downsampling halves the size of the feature maps obtained when computing the output feature map. A parallel dilated convolution (PDC) module was designed for feature extraction in multi-resolution and at various depths. The residual module has the same number of input feature maps and output channels.The inputs into and outputs from this module share the same number of feature maps as the residual module. The number of output channels as well as the size of the output feature map are the same as the first downsampling layer. A concatenation node connected the output of the parallel dilated convolution module and output of the 1st downsample layer. For simplicity, we named the above module as module 1, which consists of our designed residual module, parallel dilated convolution module, and downsampling layer. Then we built module 2, having the same parallel dilated convolution module, residual module and downsampling layer as module 1 but with a much lower dilated module rate, which enabled us to extract low frequency information. The content of module 2 is very similar to that of module 1.

Feature information from out module 2 feature map my extracted with help of designed Residual Module.

After this, an upsampling layer and regular convolution layer with LeakyReLU activation function was added to expand the "feature map" and conduct later changes in the number of output channels. To minimize information loss in upsampling, we used concatenation operation to join the output feature map of the LeakyReLU activation function and module1's output feature map.

Then, we used the proposed residual module to obtain the detailed information of the fused feature map. Further, flowing shallow features together and extracting deeper features was carried out by using the upsampling layer, standard convolution with LeakyReLU as the activation function, and the short connection and residual module.

We utilized a standard convolution followed by a Tanh activation function, to adjust the number of output channels to 3 in order to make the model output a weight for each pixel. At last we multiplied the weight-component by the attention map to do addition to the original low-light image to get the enhanced image.

1) Residual Module and Hybrid Attention

The residual module we designed combines a hybrid attention module to extract features in our designed generator. This design encoding not only is able to extract deep features, but also avoids the problems of a single feature gradient disappearing and exploding.

This designed residual module contains two sub-modules of hybrid attention module, a LeakyReLU activation function, a standard convolution module, and a skip connection. More appropriate to extract more feature information, it also enhances the correlation of different information.

The hybrid attention part is extracted out of the other residual module (2). Attention in the channel is based on global average pooling, convolution and sigmoid gate. This is pixel attention, which employs a convolution with LeakyReLU, as well as a linear convolution and a sigmoid gate. In both branches the original feature tensor is weighted; and their outputs are summed. A skip path is maintained within the residual module, allowing for preservation of a feature representation linked to inputs and maintained for aligned inputs.

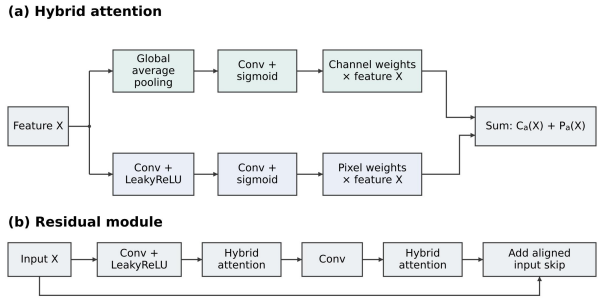


Figure 2. Hybrid channel-pixel attention and its use within the residual module.

For an intermediate tensor X, the attention outputs are C_a and P_a. These names distinguish pixel attention from the low-light image P, and distinguish hybrid attention from the generator. The following equations retain the branch operations described in the architecture:

$$H_a(X) = C_a(X) + P_a(X) \quad (6)$$

$$C_a(X) = X \odot \sigma(\text{Conv}_2(\text{Pool}(X))) \quad (7)$$

$$P_a(X) = X \odot \sigma(\text{Conv}_2(\text{Conv}_1(X))) \quad (8)$$

Here the first convolution in the pixel branch includes LeakyReLU; the second convolution is linear. Sigmoid bounds each attention weight between zero and one. For channel k, global average pooling is

$$\text{Pool}(X_k) = \frac{1}{HW}\sum_{u=1}^{H}\sum_{v=1}^{W} X_k(u, v) \quad (9)$$

Pooling reduces each H-by-W channel to a scalar value, where the weights influence the entire content. Unfortunately, the pixel branch preserves spatial structure and thus the generator is able to highlight the detailed and poorly illuminated areas.

2) Parallel Dilated Convolution

In the generator from figure 1 some features will be lost due to down-sampling. Based on the premise of reducing information loss and extracting information of low frequencies can be extracted to different scales, a parallel dilated convolution module is designed. From this module there are three parallel dilated convolutions with dilated rates of 1, 3 and 5 and a non dilated convolution layer. Dilated convolutional networks have higher receptive fields than standard-convolution networks with the same length of convolution kernel size. This can help to gain more effective low frequency information. The structure of the parallel dilated convolution module is shown in Figure 3.

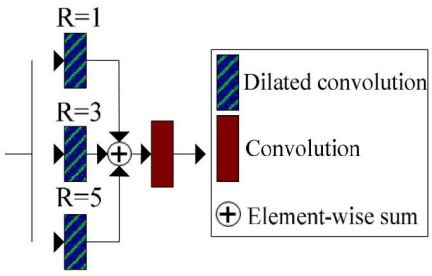


Figure 3. Element-wise Branch Fusion and parallel dilated convolution with dilation rates 1, 3 and 5.

The elementwise-sum fusion that is used in Figure 3 is as follows using r as the dilation rate. For each parallel branch output it is required that each output be of the same spatial size, and that the number of outputs match the number of intput for the subsequent Connected Encoder Decoder.

$$M(X) = \mathrm{Conv}(\mathrm{DilConv}_1(X) + \mathrm{DilConv}_3(X) + \mathrm{DilConv}_5(X)) \quad (10)$$

C. Proposed Discriminators

It is the discriminator who decides which is the image being input, the enhancement image or the original image obtained from the normal-light image. You can use it to enhance the recovery of images in generative networks based on the interaction between generator and the discriminator. For better discrimination on the part of the discriminator, the discriminator presented in table 4 was designed. There are two Discriminators in this discriminator, the Global Discriminator and the Local Discriminator. The global discriminator is a standard 4 Conv. with LeakyReLU Residual module. The residual module is three cascaded 3 × 3 dilated convolutions, each with a rate of 2, 3 and 5 respectively. With the aid of dilated convolutions, the receptive field of discriminator is expanded with a non-elevated number of parameters. The improvement in discriminative ability is obtained by having a more contextual knowledge of the input image. Also, a skip connection is added to reduce the loss of any pixels in the cascaded dilated convolution.

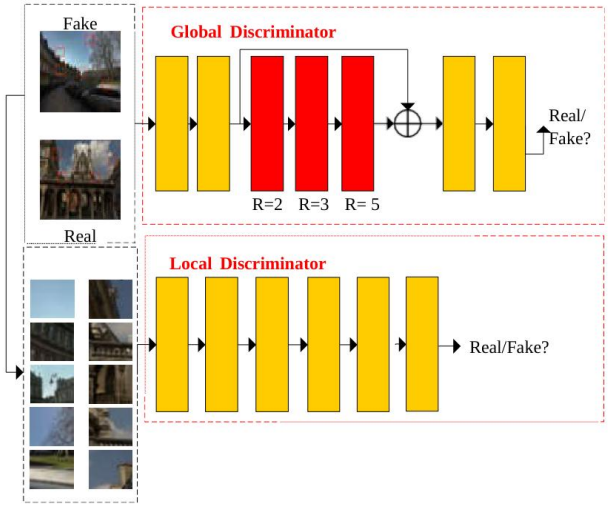


Figure 4. Global discriminator with cascaded dilation rates 2, 3, and 5 and a six-layer local discriminator.

The input image of the global discriminator was randomly cropped into patches and input to the local discriminator. It can decrease the underexposed or overexposed boosted image. Both our global discriminator and our local discriminator share the structure of the Markovian discriminator, which can gain more information from the image, and can enhance the discriminative ability of original high quality images and generated high quality images.

The global score D_g is computed from a complete image; the local score D_l is computed from patches selected by T_ω. The crop coordinates define a patch distribution independent of image pairing. For a Markovian discriminator that returns multiple scores, the squared adversarial error is averaged across its score map.

D. Proposed Loss Functions

The generator objective is multi-objective which consists of both global and local least-squares

adversarial terms with perceptual content preservation and pixel consistency terms. The discriminator objective is optimized by itself. The equation's ADD weights are retained at value 1 and no new weighting values are assumed as in stated loss.

$$L_G = L_{G,g} + L_{G,l} + L_{\text{perc}} + L_{\text{pixel}} \quad (11)$$

$$L_D = L_{D,g} + L_{D,l} \quad (12)$$

For the global generator loss, low-light samples follow p_{low}, their enhanced outputs are $\widehat{R}$, and the target discriminator score is one:

$$L_{G,g} = \mathbb{E}_{P\sim p_{\text{low}}}[(D_g(\widehat{R}) - 1)^2] \quad (13)$$

A global discriminator is used to label output as normal lights vs. detached generated output; this discriminator update is prevented from changing the parameters of the generator with stopgrad.

$$L_{D,g} = \mathbb{E}_{Y\sim p_{\text{real}}}\left[(D_g(Y) - 1)^2\right] + \mathbb{E}_{P\sim p_{\text{low}}}\left[D_g\left(\text{stopgrad}\left(\widehat{R}\right)\right)^2\right] \quad (14)$$

The local losses corresponding are applied to smaller patches, moments are expected over sampled images and crop coordinates:

$$L_{G,l} = \mathbb{E}_{P,\omega}[(D_l(T_\omega(\widehat{R})) - 1)^2] \quad (15)$$

$$L_{D,l} = \mathbb{E}_{Y,\omega}\left[(D_l(T_\omega(Y)) - 1)^2\right] + \mathbb{E}_{P,\omega}\left[D_l\left(T_\omega\left(\text{stopgrad}\left(\widehat{R}\right)\right)\right)^2\right] \quad (16)$$

Perceptual loss computes the loss of the generated output from the lower light input, based on the features extracted in the pre-trained, frozen VGG16 network of the problem. ϕ_(i,j) means the jth convolution in block i and H_(i,j) and W_(i,j) are the horizontal and vertical sizes of the convolution, respectively. The vector norm can be applied in the computation of feature difference as the sum of squares of differences across channels for a spatial location.

$$L_{\text{perc}} = \frac{1}{H_{i,j}W_{i,j}}\sum_{u=1}^{H_{i,j}}\sum_{v=1}^{W_{i,j}} \|\phi_{i,j}(\widehat{R})_{u,v} - \phi_{i,j}(P)_{u,v}\|^2 \quad (17)$$

It takes flattened entries of RGB for m = 3HW pixels that lose their consistency. It isn't a supervised loss to an unpaired normal-light training image, but does bound the deviation from the original image.

$$L_{\text{pixel}} = \sum_{i=1}^{m}(P_i - \widehat{R}_i)^2 \quad (18)$$

The former terms preserve information about the contents of the scene while the latterterms promote normal-light look. The unnormalized pixel sum and the loss for the features have different numerical scales, which affects the balance of these two and thus the degree of change in illumination that is possible to achieve.

E. Training and Inference Algorithms

The alternating global/local adversarial training procedure is specified in Algorithm 1 and inference with a trained generator only is specified in Algorithm 2. Both contain numbers in their statements, explicit inputs and outputs, and indented control blocks. The collection of the low-light data set is independent from the collection of the normal-light data set (minibatch sampling).

The reported learning-rate schedule has initial rate η_0 = 0.0001, total epochs E = 200, and a 100-epoch hold period. For epoch e from 1 to 200, the following expression gives a constant rate for the first 100 epochs and linear decay thereafter:

$$\eta_e = \eta_0 \min(1, \tfrac{200-e}{100}) \quad (19)$$

Algorithm 1: Alternating training of the low-light enhancement GAN.

Input: Unpaired image collections; initialized θ_G, θ_g, θ_l; frozen VGG16 features; E = 200; b = 4; η_0 = 0.0001; β_1 = 0.5; β_2 = 0.999.

Output: Trained generator parameters θ_G.

1: Initialize independent Adam optimizer states for the generator and both discriminators.

2: **for** e = 1 to E do

3: Set η_e from Eq. (19) in all three optimizers.

4: **for** each training minibatch do

5: Sample independent minibatches B_{low} and B_{real}, each with b images.

6: Compute I, A, and the enhanced outputs $\widehat{R}$ using Eqs. (3)-(5).

7: Draw crop coordinates and apply T_{ω} to real and enhanced images.

8: Detach generated outputs from the generator computation graph.

9: Compute $L_{D,g}$ and $L_{D,l}$ using Eqs. (14) and (16).

10: Clear discriminator gradients; backpropagate L_D.

11: Update θ_g and θ_l with their Adam optimizers.

12: Freeze discriminator parameters without disabling gradients to generator outputs.

13: Recompute $\widehat{R}$ with the generator graph enabled.

14: Compute $L_{G,g}$, $L_{G,l}$, L_{perc}, and L_{pixel}.

15: Sum the four terms to obtain L_G using Eq. (11).

16: Clear generator gradients; backpropagate L_G.

17: Update θ_G with the generator Adam optimizer.

18: Unfreeze the discriminator parameters.

19: **end for**

20: **end for**

21: **return** θ_G.

Algorithm 2: Generator-only enhancement of a low-light image.

Input: Low-light RGB image P; trained parameters θ_G; the same luminance normalization used for training.

Output: Enhanced RGB image $\widehat{R}$ with the input spatial dimensions.

1: Load the parameters for the generator and set the generator to evaluation mode.

2: Turn off recording of parameter-gradients for inference.

3: Calculate the normalized luminance I and attention A in terms of dark regions.

4: Send A to the RGB channel (broadcast A), make the generator input from Eq. (4).

5: Run encoder and attention residual blocks, and parallel dilated convolutions.

6: Run the decoder using the upsampling and the concatenation of encoder-decoder skip.

7: Compute the three-channel Tanh residual and reconstruct $\widehat{R}$ by Eq. (5).

8: **return** $\widehat{R}$; do not run the discriminators.

IV. SIMULATION AND DISCUSSION

We compare the proposed method with a number of other recently published methods including Alpha-rooting, LIME, CycleGAN, Retinex-Net, EnlightenGAN, Zero-DCE, and Zero-DCE++. Construction, normal-light images, require aligned normal-light images as reference to obtain scores for PSNR and SSIM, while both NIQE and BRISQUE make no-reference assessments. The provided the training configuration uses batch size 4, Adam Adam1 and Adam2 0.5 and 0.999 respectively, and 200 epochs. Part 100: Learning Rate: 0.0001; for the first 100 epochs, the learning rate stays as 0.0001 and goes linear to 0 afterward. The training procedure is described by Algorithm 1 below. The claimed implementation includes the Ubuntu 18.04 operating system, NVIDIA 2080 Ti GPU, and PyTorch.

A. Datasets and Evaluation Metrics

Low-light images are described in [22] as part of an unpaired training collection with 914 images at the stated resolution of 600×400 pixels, whereas the collection of normal-light images consists of 1,016 images. The 150 low-light images chosen for the test set are taken from SICE [33] with no reference images. The full-reference evaluation is based on the LOL collection of 500 image pairs of low-light and normal-light images. The paired normal-light reference should match the tested input image and same reference/scene and same pixel position.

NIQE models natural scene statistics as multivariate Gaussian. Suppose the "natural-image" model has mean and covariance identified by 1 and the "enhanced-test-image" model is identified by 2. Their covariance-normalized statistical distance is called NIQE:

$$\text{NIQE} = \sqrt{(\mu_1 - \mu_2)^T \left(\frac{\Sigma_1 + \Sigma_2}{2}\right)^{-1} (\mu_1 - \mu_2)} \quad (20)$$

Smaller NIQE score means that it is closer to natural image statistics. During the assessment for BRISQUE, J is an image used for gray images in sampling local mean and local standard deviation. Coefficients that take into account the effects of mean subtraction and contrast normalization.

$$\hat{J}(u,v) = \frac{J(u,v) - \mu_J(u,v)}{\sigma_J(u,v) + \varepsilon}, \quad \varepsilon > 0 \quad (21)$$

BRISQUE does not offer the MSCN coefficient; it is just a tool that can be used to provide feedback regarding the coefficient. It derives statistical features at multiple scales by applying a learned support-vector regressor [32] to distributions of MSCN coefficients and neighbouring products. The better the predicted image quality, the lower the BRISQUE score:

$$\text{BRISQUE}(J) = f_{\text{SVR}}(\Psi_{\text{NSS}}(J)) \quad (22)$$

PSNR is defined based on mean squared error with an aligned reference Y and an enhanced output, m = 3HW is a scalar RGB inputs. The range (1 or 255) should match that of the data, one for normalized intensities, 255 for 8-bit intensities.

$$\text{MSE} = \frac{1}{m}\sum_{i=1}^{m} (Y_i - \hat{R}_i)^2 \quad (23)$$

$$\text{PSNR} = 10 \log_{10}\left(\frac{L_{\max}^2}{\text{MSE}}\right) \quad (24)$$

SSIM computes both the local luminance, contrast and structure between reference and output aligned windows. The Y-subscript and R-subscript refer to local means, variances and covariance. The ratios are held stable by the positive constants and an image score takes the average of the ratios over the local area.

$$\text{SSIM} = \frac{(2\mu_Y\mu_R + C_1)(2\sigma_{YR} + C_2)}{(\mu_Y^2 + \mu_R^2 + C_1)(\sigma_Y^2 + \sigma_R^2 + C_2)} \quad (25)$$

Better agreement to the reference is manifested by the higher PSNR and SSIM. The direction of NIQE and BRISQUE are opposite. Therefore the tables refer to every one of the metric directions and the heatmaps rescale each metric row independently to meaningfully categorize each one by a darker cell representing a better performance. The colors of the heatmap provided are not an actual composite grade.

B. Ablation Study

The complete model and four models based on the above-mentioned complete full-reference image sets are evaluated, namely the removal of the hybrid attention, parallel dilated convolution, cascaded dilated convolution in the global discriminator, or pixel loss. The reported scores are in the context of Table 2. The complete model performs best with the highest PSNR and SSIM, as well as the lowest NIQE and BRISKE scores. The highest PSNR value decreases from 26.6451 to 20.5918 dB when the attention is removed. The nan pixels are added to BRISQUE and affect it significantly as compared to PSNR, which is relatively not affected.

Table 2. Ablation results for the proposed network.

Model variant	PSNR (dB) ↑	SSIM ↑	NIQE ↓	BRISQUE ↓
Without hybrid attention	20.5918	0.7686	6.7748	25.3088
Without parallel dilated convolution	23.3964	0.7761	5.2070	22.2576
Without cascaded dilated convolution	25.9701	0.8667	4.8803	21.5149
Without pixel loss	26.1541	0.8771	4.9612	40.0626
Complete model	**26.6451**	**0.8817**	**4.4719**	**21.2218**

Better direction shown by arrows. Bold values indicate the full model; all scores are kept to the same precision as specified above.

These ablation scores are shown in figure 5. Here colored cells indicate within-column min-max performance after reversing NIQE and BRISQUE; gray cells show the original NIQE values and the various colors indicate the differents between the min-max values. These results provide evidence of the contribution of each component to the

evaluation set forth; they are not indicative of statistical significance or robustness to unseen datasets.

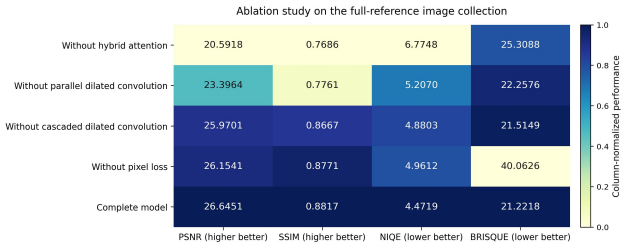


Figure 5. Ablation heatmap. Raw metric values are annotated; darker cells denote better within-column performance.

C. No-Reference Image Quality Assessment

The NIQE and BRISQUE scores of the four exemplar images published in the manuscript is summarized in Tables 3 and 4. The proposed method has the lowest values of NIQE on all four examples including its mean NIQE value (4.4382). It achieves the lowest BRISQUE scores with three of four examples, and the lowest mean BRISQUE score below 24.8455. The proposed method would compare favorably with the BRISQUE score of EnlightenGAN 30.4125 on Image 1, which is slightly higher than the proposed method 30.5261, however, the proposed method is not better on all of the metrics and exemplars.

Table 3. NIQE scores for four exemplar images.

Method	Image 1	Image 2	Image 3	Image 4	Reported mean
Alpha-rooting	6.9561	7.1162	8.2354	8.3671	7.6687
LIME	6.6348	4.7842	8.3674	6.3724	6.5397
CycleGAN	7.5064	5.8236	6.5934	7.6354	6.8897
Retinex-Net	12.4557	6.7309	10.6873	11.3648	10.3097
EnlightenGAN	5.2253	3.6692	5.2263	4.6992	4.7050
Zero-DCE	8.8149	5.1637	6.3784	4.4762	6.2083
Zero-DCE++	7.8973	4.5945	6.1283	4.1164	5.6841
Proposed method	**5.1815**	**3.4426**	**5.1637**	**3.9651**	**4.4382**

The lower the score the better. The mean value reported shows the original numbers rounded, bold indicates the suggested approach.

Table 4. BRISQUE scores for four exemplar images.

Method	Image 1	Image 2	Image 3	Image 4	Reported mean
Alpha-rooting	42.6327	41.2961	36.1284	39.6183	39.9189
LIME	43.6249	40.4375	37.9658	50.5563	43.1461
CycleGAN	38.6523	40.1263	28.1267	36.2548	35.7900
Retinex-Net	44.2361	48.2763	38.1476	53.2174	45.9694
EnlightenGAN	30.4125	29.1547	23.6321	35.2147	29.6035
Zero-DCE	36.2578	30.1542	29.3697	40.1236	33.9763
Zero-DCE++	33.6245	28.7163	24.3698	29.7211	29.1079
Proposed method	**30.5261**	**20.5238**	**22.9086**	**25.4236**	**24.8455**

The lower the score the better. Table shows mean value reported with original rounded value, bold indicates proposed method.

For the given no-reference evaluation collection – for the whole collection – all eight methods return the same mean NIQE and BRISQUE results for this collection, reported in the corresponding rows of Table 5. The proposed method has the lowest values for both metrics: NIQE 4.8656 and BRISQUE 23.6987. The second comes from EnlightenGAN with score 5.2901 for NIQE, while the second is obtained by the algorithm Zero-DCE for BRISQUE, which is 24.3687. Therefore, the basic ranking is based upon the quality function.

Table 5. Mean no-reference quality scores over the stated evaluation collection.

Method	NIQE ↓	BRISQUE ↓
Alpha-rooting	8.8655	41.0368
LIME	8.9884	40.3652
CycleGAN	8.8816	39.6235
Retinex-Net	7.8564	41.3498
EnlightenGAN	5.2901	30.2563
Zero-DCE	6.1564	28.6392
Zero-DCE++	5.7911	24.3687
Proposed method	**4.8656**	**23.6987**

These are reported at the method level, not at the image observation level.

The mean score pairs displayed in figure 6 are the ones from table 5. Better NIQE and BRISQUE are represented in the lower left corners. The proposed method is to be carried out in this favorable region. These eight aggregate observations do not imply regression line nor imagelevel correlation.

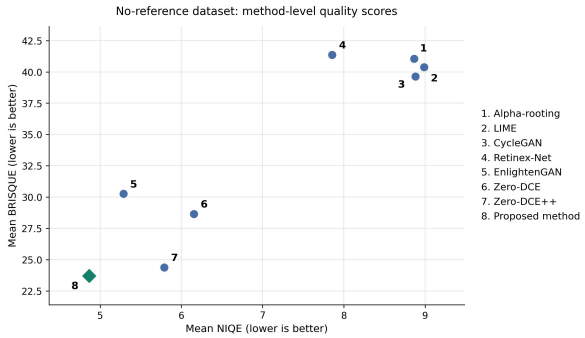


Figure 6. Scatter plot of mean NIQE against mean BRISQUE for eight methods on the no-reference collection.

D. Full-Reference Image Quality Assessment

Table 6 gives PSNR, SSIM, NIQE and BRISQUE of three reported exemplar images with each performance measure displayed in an editable row. The highest PSNR and the lowest NIQE and BRISQUE methods are those with the proposed method on all three examples. Indeed, it is not always best for SSIM as in the case of Image 3, the EnlightenGAN has SSIM 0.8802 compared to 0.8695 for the proposed method. Hence the comparison regards the joint metric profile and not the best performance for every component individual.

Table 6. Per-image scores and arithmetic means for three full-reference exemplar images.

	Method	PSNR (dB) ↑	SSIM ↑	NIQ
	Alpha-rooting	20.1381	0.8032	5.9
	LIME	19.8378	0.7732	6.9
	CycleGAN	23.0964	0.7944	7.2
	Retinex-Net	15.9278	0.7839	7.5
	EnlightenGAN	21.8685	0.9213	4.9
	Zero-DCE	15.9880	0.8529	5.0
	Zero-DCE++	15.4431	0.6098	4.9
	Proposed method	**24.1329**	**0.9267**	**4.7**
	Alpha-rooting	19.6382	0.7886	7.0
	LIME	17.9721	0.7770	8.2
	CycleGAN	19.8103	0.8515	8.2
	Retinex-Net	13.2096	0.7312	6.2
	EnlightenGAN	23.2018	0.9208	3.9
	Zero-DCE	16.5817	0.8294	4.9
	Zero-DCE++	16.3813	0.7320	4.6
	Proposed method	**27.3032**	**0.9352**	**3.8**
	Alpha-rooting	18.6357	0.7081	9.0
	LIME	17.3886	0.6572	7.6354
	CycleGAN	19.0584	0.6837	9.6102
	Retinex-Net	15.8160	0.6637	5.1632
	nlightenGAN	17.3886	0.8802	5.1022
	Zero-DCE	17.2072	0.7673	5.8906
	Zero-DCE++	18.8322	0.6311	5.1063
	oposed method	**20.5577**	**0.8695**	**4.9924**
	lpha-rooting	19.4707	0.7666	7.7733
	LIME	18.3995	0.7358	7.6547
	CycleGAN	20.6550	0.7765	8.3616
	Retinex-Net	14.9845	0.7263	6.3317
	nlightenGAN	20.8196	0.9074	4.6871
	Zero-DCE	16.5923	0.8165	5.3013
	Zero-DCE++	16.8855	0.6576	4.9110
	oposed method	**23.9979**	**0.9105**	**4.5472**

Mean rows are the arithmetic average for each of the three scores shown per image. These do not look at data from any of the other dimensions in the dataset and as a result are not part of Table 7 (Data View, Table-wide). The source table value is maintained in each per image score.

The reported aggregates for the specified complete reference sample set are provided in Table 7. The proposed method has the highest PSNR (26.6451 dB) and SSIM (0.8817), and the lowest NIQE (4.4719) and BRISQUE (21.2218). EnlightenGAN has the 2nd rank on every following 4 aggregate measures. The results in Table 7 are for the entire collection and are not the same as each of the three arithmetic means shown in Table 6.

Table 7. Mean quality scores over the stated full-reference evaluation collection.

Method	PSNR (dB) ↑	SSIM ↑	NIQE ↓	BRISQUE ↓
Alpha-rooting	17.3354	0.7022	8.9621	39.6477
LIME	17.8337	0.6321	8.9673	40.3188
CycleGAN	21.1463	0.8322	8.1960	30.3485
Retinex-Net	17.7947	0.6257	6.9928	34.5698
EnlightenGAN	23.9674	0.8640	4.8963	23.2056
Zero-DCE	19.7008	0.7416	6.0023	29.4853
Zero-DCE++	18.8698	0.6463	5.3725	24.8423
Proposed method	**26.6451**	**0.8817**	**4.4719**	**21.2218**

The larger the PSNR/SSIM, and the smaller the NIQE/ BRISQUE are, the better. The bold marks indicate the suggested approach. The reported aggregates are unchanged.

Results were shown in figure 7, which depicts the mean PSNR and the mean of the SSIM for each of the 6 methods of Table 7. The upper-right corner of the proposed method shows high fidelity for aggregates and resemblance with the structure. Figure 8 presents all four reported metrics as independent column normalization—in this case the values on the figure are annotated so that the raw results may be compared to the results in Table 7.

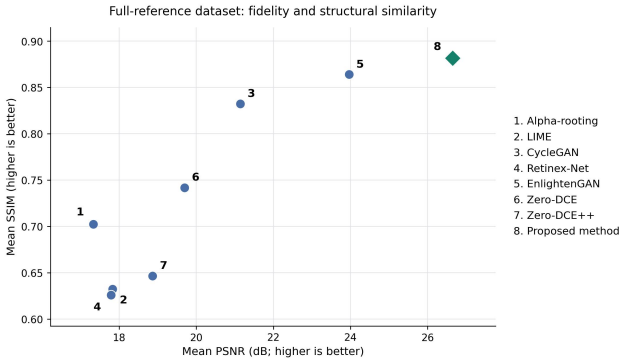


Figure 7. Scatter plot of mean PSNR against mean SSIM for eight methods on the full-reference collection.

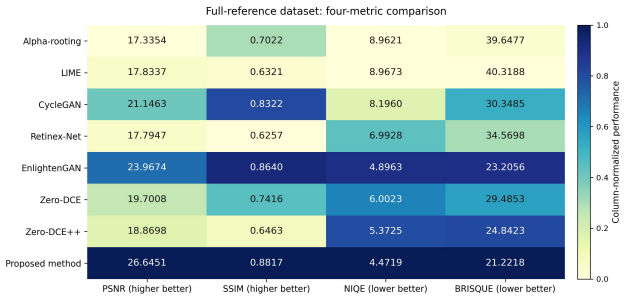


Figure 8. Full-reference benchmark heatmap. Raw values are annotated and metric colors are normalized separately.

V. CONCLUSION

In this paper, a novel unsupervised low-light image enhancement method based on generative adversarial network is proposed. The generator uses the residual module, a hybrid attention module, a parallel dilated convolution module and a skip connection that can help to capture high-frequency and low-frequency information from the input image. Our discriminator is composed of a discriminator called discriminator, which is based on the same idea of a Markovian discriminative network but extends it to deal with discriminator on a global scale. One of the key design elements in our network is that it can capture both the global and local image characteristics. In order to better develop the discriminative power of the discriminator in the whole world, three cascade dilated convolutions with larger receptive field are introduced. The paper proposes to enhance this loss function by adding the pixel loss to the loss function of the generative adversarial network, which is demonstrated to be a better strategy to enhance the enhancement performance. The addition assists in restoring more information in the improved images. The proposed model is tested on a full-reference and no-reference sets and extensive experimental results show its performance superiority compared to seven existing methods for low light image enhancement.

REFERENCES

. Dai, Y.; Liu, W. GL-YOLO-Lite: A Novel Lightweight Fallen Person Detection Model. Entropy, 2023, 25, 587.

. Wang, H.; Chen, Y.; Cai, Y.; Chen, L.; Li, Y.; Sotelo, M.A.; Li, Z. SFNet-N: An Improved SFNet Algorithm for Semantic Segmentation of Low-Light Autonomous Driving Road Scenes. IEEE Transactions on Intelligent Transportation Systems, 2022, 23, 21405–21417.

. Lim, S.; Kim, W. DSLR: Deep Stacked Laplacian Restorer for Low-Light Image Enhancement. IEEE Transactions on Multimedia, 2021, 23, 4272–4284.

4. Veluchamy, M.; Bhandari, A.K.; Subramani, B. Optimized Bezier Curve Based Intensity Mapping Scheme for Low Light Image Enhancement. IEEE Transactions on Emerging Topics in Computing, 2021, 6, 602–612.
5. Chen, Y.-S.; Wang, Y.-C.; Kao, M.-H.; Chuang, Y.-Y. Deep Photo Enhancer: Unpaired Learning for Image Enhancement from Photographs with GANs. In Proceedings of the IEEE/CVF Conference on Computer Vision and Pattern Recognition, Salt Lake City, UT, USA, 18-23 June 2018, pp. 6306–6314.
6. Shi, Y.; Wang, B.; Wu, X.; Zhu, M. Unsupervised Low-Light Image Enhancement by Extracting Structural Similarity and Color Consistency. IEEE Signal Processing Letters, 2022, 29, 997–1001.
7. Lin, Y.; Lu, Y. Low-Light Enhancement Using a Plug-and-Play Retinex Model with Shrinkage Mapping for Illumination Estimation. IEEE Transactions on Image Processing, 2022, 31, 4897–4908.
8. Ren, X.; Yang, W.; Cheng, W.-H.; Liu, J. LR3M: Robust Low-Light Enhancement via Low-Rank Regularized Retinex Model. IEEE Transactions on Image Processing, 2022, 29, 5862–5876.
9. Wei, C.; Wang, W.; Yang, W.; Liu, J. Deep Retinex Decomposition for Low-Light Enhancement. arXiv, 2018, arXiv:1808.04560.
10. Yang, W.; Wang, S.; Fang, Y.; Wang, Y.; Liu, J. From Fidelity to Perceptual Quality: A Semi-Supervised Approach for Low-Light Image Enhancement. In Proceedings of the IEEE/CVF Conference on Computer Vision and Pattern Recognition (CVPR), Seattle, WA, USA, 13-19 June 2020, pp. 3060–3069.
1. Guo, C.; Li, C.; Guo, J.; Loy, C.C.; Hou, J.; Kwong, S.; Cong, R. Zero-Reference Deep Curve Estimation for Low-Light Image Enhancement. In Proceedings of the Conference on Computer Vision and Pattern Recognition (CVPR), Seattle, WA, USA, 13-19 June 2020, pp. 1777–1786.
2. Li, C.; Guo, C.; Chen, C.L. Learning to Enhance Low-Light Image via Zero-Reference Deep Curve Estimation. IEEE Transactions on Pattern Analysis and Machine Intelligence, 2021, 44, 4225–4238.
3. Lv, T.; Pan, X.; Zhu, Y.; Li, L. Unsupervised Medical Images Denoising via Graph Attention Dual Adversarial Network. Applied Intelligence, 2021, 51, 4094–4105.
4. Li, X.; Wu, Y.; Zhang, W.; Wang, R.; Hou, F. Deep Learning Methods in Real-Time Image Super-Resolution: A Survey. Journal of Real-Time Image Processing, 2020, 17, 1885–1909.
5. Ha, V.K.; Ren, J.; Xu, X.; Liao, W.; Zhao, S.; Ren, J.; Yan, G. Optimized Highway Deep Learning Network for Fast Single Image Super-Resolution Reconstruction. Journal of Real-Time Image Processing, 2020, 17, 1961–1970.
6. Ren, Z.; Zhang, Y.; Wang, S. A Hybrid Framework for Lung Cancer Classification. Electronics, 2022, 11, 1614.
7. Hua, W.; Xia, Y. Low-Light Image Enhancement Based on Joint Generative Adversarial Network and Image Quality Assessment. In Proceedings of the 11th International Congress on Image and Signal Processing, BioMedical Engineering and Informatics, Beijing, China, 13-15 October 2018, pp. 1–6.
8. Kim, G.; Kwon, D.; Kwon, J. Low-LightGAN: Low-Light Enhancement via Advanced Generative Adversarial Network with Task-Driven Training. In

Proceedings of the International Conference on Image Processing, Taipei, Taiwan, 22-25 September 2019, pp. 2811–2815.
19. Shi, Y.; Wu, X.; Zhu, M. Low-Light Image Enhancement Algorithm Based on Retinex and Generative Adversarial Network. arXiv, 2019, arXiv:1906.06027.
20. Guo, L.; Wan, R.; Su, G. Multi-Scale Feature Guided Low-Light Image Enhancement. In Proceedings of the International Conference on Image Processing, Anchorage, AK, USA, 19-22 September 2021, pp. 554–558.
21. Yang, S.; Zhou, D.; Cao, J.; Guo, Y. Rethinking Low-Light Enhancement via Transformer-GAN. IEEE Signal Processing Letters, 2022, 29, 1082–1086.
22. Jiang, Y.; Gong, X.; Liu, D.; Cheng, Y.; Fang, C.; Shen, X.; Yang, J.; Zhou, P.; Wang, Z. EnlightenGAN: Deep Light Enhancement Without Paired Supervision. IEEE Transactions on Image Processing, 2021, 30, 2340–2349.
23. Li, F.; Zheng, J.; Zhang, Y. Generative Adversarial Network for Low-Light Image Enhancement. IET Image Processing, 2021, 15, 1542–1552.
24. Qu, Y.; Chen, K.; Liu, C.; Ou, Y. UMLE: Unsupervised Multi-Discriminator Network for Low-Light Enhancement. In Proceedings of the International Conference on Robotics and Automation, Xi'an, China, 30 May–5 June 2021, pp. 4318–4324.
25. Rao, N.; Lu, T.; Zhou, Q. Seeing in the Dark by Component-GAN. IEEE Signal Processing Letters, 2021, 28, 1250–1254.
26. Grigoryan, A.M.; Agaian, S.S. Alpha-Rooting and Correlation Method of Image Enhancement. Multimodal Image Exploitation and Learning, 2022, 12100, 147–156.
7. Guo, X.; Li, Y.; Ling, H. LIME: Low-Light Image Enhancement via Illumination Map Estimation. IEEE Transactions on Image Processing, 2017, 26, 982–993.
8. Zhu, J.Y.; Park, T.; Isola, P.; Efros, A.A. Unpaired Image-to-Image Translation Using Cycle-Consistent Adversarial Networks. In Proceedings of the IEEE International Conference on Computer Vision (ICCV), Venice, Italy, 22-29 October 2017, pp. 2223–2232.
9. Appina, B. A 'Complete Blind' No-Reference Stereoscopic Image Quality Assessment Algorithm. In Proceedings of the 2020 International Conference on Signal Processing and Communications (SPCOM), Bangalore, India, 19-24 July 2020, pp. 1–5.
0. Alqawasmi, K. Estimation of ARMA Model Order Utilizing Structural Similarity Index Algorithm. In Proceedings of the 8th International Conference on Control, Decision and Information Technologies, Istanbul, Turkey, 17-20 May 2022, pp. 1087–1090.
1. Javaheri, A.; Brites, C.; Pereira, F.; Ascenso, J. Improving PSNR-Based Quality Metrics Performance for Point Cloud Geometry. In Proceedings of the 27th International Conference on Image Processing (ICIP 2020), Abu Dhabi, United Arab Emirates, 25-28 October 2020, pp. 3438–3442.
2. Mittal, A.; Moorthy, A.K.; Bovik, A.C. No-Reference Image Quality Assessment in the Spatial Domain. IEEE Transactions on Image Processing, 2012, 21, 4695–4708.
3. Cai, J.; Gu, S.; Zhang, L. Learning a Deep Single Image Contrast Enhancer from Multi-Exposure

Images. IEEE Transactions on Image Processing, 2018, 27, 2049–2062.
34. W. Yu, L. Zhao, and T. Zhong, "Unsupervised Low-Light Image Enhancement Based on Generative Adversarial Network," Entropy, vol. 25, no. 6, article 932, 2023. doi: 10.3390/e25060932.